Radiation Physics and Chemistry 232 (2025) 112666

Contents lists available at ScienceDirect

Radiation Physics and Chemistry

journal homepage: www.elsevier.com/locate/radphyschem

ANN-driven unfolding of epithermal neutron spectra in variable-geometry beam-shaping assemblies

S. Bedenko [a,*], S. Polozkov [a], G. Vlaskin [b], N. Ghal-Eh [c], F. Rahmani [d], D. Veretennikov [a], S. Bagherzadeh-Atashchi [c]

[a] School of Nuclear Science and Engineering, National Research Tomsk Polytechnic University, 634050, Tomsk, Russian Federation
[b] Proryv JSC, Rosatom, 119017, Moscow, Russian Federation
[c] Department of Physics, Faculty of Science, Ferdowsi University of Mashhad, 91775-1436, Mashhad, Iran
[d] Department of Physics, K. N. Toosi University of Technology, 16315-1618, Tehran, Iran

ARTICLE INFO

Handling Editor: Chris Chantler

Keywords:
Fast (α, n) neutron beams
^{2,3}H fusion and (α, n) reactions
Variable-geometry beam-shaping assembly
Unfolding of the neutron spectrum
Artificial neural networks

ABSTRACT

To study the risks associated with neutron fields from various sources, direct measurements using advanced detection technologies are essential. This study explores the Thermal Neutron Imaging System (TENIS) for characterizing the energy spectrum of an (α, n) neutron beam generated in the collimated channel of the Prizm-AN facility utilizing an IBN-10 source. We present the performance characteristics of the neutron beam, the permissible operational duration near the installation, a comprehensive map of thermal neutron flux parameters, and the results of spectrum unfolding achieved using artificial neural networks (ANNs). Our analysis confirms that TENIS can effectively measure the energy spectrum of slowed-down (α, n) neutrons produced under horizontal collimation. Additionally, we highlight the similarities between ^{2,3}H fusion and (α, n) reactions, integrating the Prizm-AN complex with TENIS as a powerful tool for the real-time monitoring and control of plasma parameters within the paired plasma source neutrons (PSN) and variable-geometry beam-shaping assembly (vBSA) system.

1. Introduction

In previous studies, the feasibility of utilizing the paired system comprising a blanket, plasma source neutrons (PSN), and a variable-geometry beam-shaping assembly (vBSA) was investigated (Bedenko et al., 2024). This approach aims to establish a radiation emission source through a linear configuration of a plasma-physical accelerator, employing a neutron pumping scheme for a solid-state active medium.

The system under study consists of an external pulsed source of neutrons (*i.e.*, D-T) based on an extended gas-dynamic magnetic trap, denoted in (Ivanov and Prikhodko, 2013) as plasma source neutrons, and a subcritical blanket (Bedenko et al., 2022) which includes a vBSA and an active medium.

Gadolinium oxide (Gd_2O_3) enriched in ^{155}Gd isotope is used as the active medium; as the main pump scheme, the channel of ^{156}Gd (^{156m}Gd) isotope formation in the inverse state is studied, the de-excitation of which is accompanied by the emission of an intense gamma-ray line with a wavelength of $\sim 10^{-4}$ nm (~12.4 MeV) (Shamanin and Kazaryan, 2017).

To achieve the required conditions for neutron pumping within the active medium, we utilize a vBSA. The vBSA is a device consisting of moderating blocks and selective plates that are specifically designed to maintain and shape a neutron beam with an epithermal spectrum (Bedenko et al., 2024).

In their 2017 study, Shamanin and Kazaryan demonstrated that the active medium is highly sensitive to the shape and parameters of the neutron field (Shamanin and Kazaryan, 2017). Consequently, it is essential to equip the vBSA with a comprehensive monitoring and control system. Integrating the vBSA with such a control system will enable real-time adjustments to the configuration of the vBSA in response to the operational mode of the D-T neutron source. This capability will facilitate the formation of a neutron beam with the desired intensity and spectrum, thus optimizing the conditions necessary for stabilizing the energy levels of the nuclei within the active medium (Shamanin et al., 2021; Bedenko et al., 2024).

An analysis of scientific and technical solutions available in (Aza et al., 2016; Ghal-Eh and Green, 2016; Yazdandoust et al., 2021; Borgwardt et al., 2022; Heshmati et al., 2022; Buffler et al., 2023;

* Corresponding author.
E-mail address: bedenko@tpu.ru (S. Bedenko).

https://doi.org/10.1016/j.radphyschem.2025.112666
Received 12 November 2024; Received in revised form 10 January 2025; Accepted 1 March 2025
Available online 4 March 2025

García-Baonza et al., 2023) showed that the ThErmal Neutron Imaging System (TENIS) equipment is best suited for integration with the vBSA (Ghal-Eh and Green, 2016; Yazdandoust et al., 2021). Moreover, the studies confirm that TENIS is well-suited for our present research objectives (Bagherzadeh-Atashchi et al., 2023; Bedenko et al., 2024).

TENIS, is a sophisticated orthogonal arrays of commercial plastic scintillators designed for real-time neutron detection and visualization of the thermal neutron map. According to the results of previous studies, the TENIS has successfully proven itself for mono- and poly-energy neutron sources (Bagherzadeh-Atashchi et al., 2023). For example, Ghal-Eh and Green (2016) and Yazdandoust et al. (2021) used the TENIS to map a thermal neutron beam inside a rectangular water phantom irradiated by an external neutron flux. In this project, TENIS becomes a tool to determine the characteristics of epithermal neutron beam in the region where the active medium is located. The scientific and technical feasibility of this possibility will be demonstrated at the Prizm-AN measurement complex with a Pu–Be (α, n) neutron source installed.

Thus, the main goal of the present project is to study the properties of the Prizm-AN installation with the TENIS device as an accessible analogue for studying the capabilities of the blanket-PSN-vBSA paired system.

The subsequent sections of this paper will present and analyze the developed Prizm-AN and Pu–Be models of the internal bounded neutron (IBN)-type source with similar spectra as PSN as well as detection systems for TENIS. Specifically, we will: (1) present the results of the emission spectrum calculations for IBN-10 neutrons; (2) compare the experimental measurements obtained from the Prizm-AN with the calculated parameters of the neutron flux within the channel and at the exit of the Prizm-AN channel; and (3) provide a map depicting the thermal neutron fluence rate parameters acquired through TENIS, along with the results of spectrum unfolding for the IBN-10 using ANNs.

It should be noted that the TENIS project with the results discussed in (Ghal-Eh and Green, 2016; Yazdandoust et al., 2021; Bagherzadeh-Atashchi et al., 2023) is in the feasibility study stage, where the full-scale studies to demonstrate the new capabilities of the TENIS equipment will be useful to the developers.

2. Materials and methods

2.1. Thermal Neutron Imaging System and PNS

TENIS is made of seventeen rectangular NE102 plastic scintillators (*i.e.,* seven 2 × 2 × 20 cm^3 horizontal and ten 2 × 2 × 14 cm^3 vertical detectors) in an orthogonal arrangement, where they are placed on both sides of the rectangular water phantom (Fig. 1).

TENIS is used to map the thermal neutron flux inside a rectangular phantom irradiated by an external neutron beam. Neutrons undergo $^1H(n_{th}, \gamma)^2D$ reactions during thermalization inside the phantom and emit 2.22 MeV γ-rays before they are registered by two orthogonal arrays of plastic scintillators. The gamma-rays detected by the scintillator system contain information about the neutron interaction location, serving as input datasets for an algorithm designed to unfold the neutron spectrum.

In this study, the thermal neutron image constructed by TENIS is used to unfold the characteristics of the neutron field in the pumping zone of the active medium where TENIS becomes a tool for monitoring and controlling the parameters of the neutron flux modulated by the multicomponent selective vBSA structure.

The scientific and technical justification of the possible use of TENIS for solving monitoring and control tasks was carried out at the Prizm-AN installation shown in Fig. 2. Prizm-AN is a measurement setup consisting of a polyethylene prism with a horizontal channel and a 250-GBq Pu–Be radioisotope capsule source of fast neutrons (Pu–Be neutron source, type IBN-10). The Prizm-AN installation is located in the Neutronic

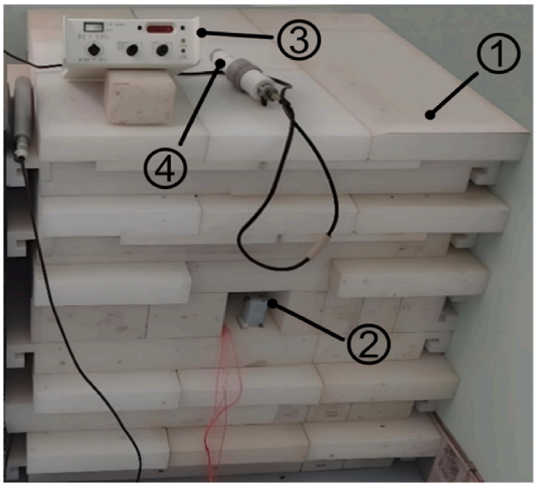

Fig. 2. Prizm-AN installation: (1) polyethylene prism with (2) Pu–Be neutron source IBN-10; (3) scintillator radiometer-dosimeter MKS-01R; (4) the ^3He neutron detection unit.

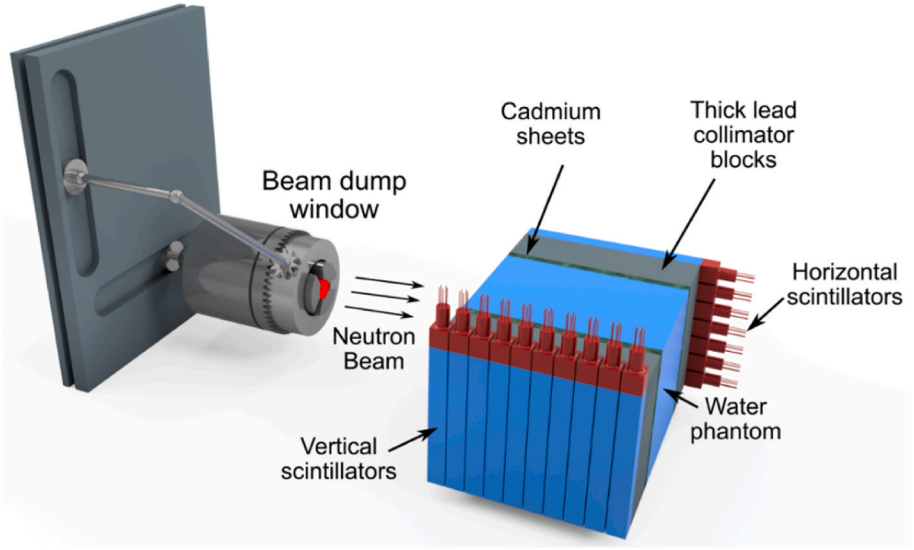

Fig. 1. Schematic representation of the vBSA beam dump window and components of the TENIS.

Measurement Laboratory of Tomsk Polytechnic University. At present, the laboratory equipped with this installation has been successfully used for conducting applied research and training in the fields of nuclear and neutron physics, neutron activation analysis, and neutron transport theory.

The analysis of results from previous studies indicates that the neutron spectrum produced by the PSN generator (Bedenko et al., 2020), particularly in the epithermal energy range, exhibits similarities to the spectrum generated by a radioisotope intermetallic source (Fig. 3). This source produces neutrons via (α, n) reactions on ^{9}Be nuclei. Consequently, our comparison highlights the parallels between fusion- and (α, n) reactions.

Based on our findings, we conclude that the Prizm-AN, equipped with the IBN-10 capsule, serves as an appropriate analogue for investigating the technical capabilities of the paired blanket-PSN-vBSA system. In conclusion, the integration of Prizm-AN with IBN-10 and TENIS will validate the technical feasibility of employing neutron spectrometry with TENIS. This approach aims to effectively monitor and control the parameters of the D-T neutron beam during the preliminary phase leading up to the design of the vBSA demonstration version.

2.2. Calculation models of Prizm-AN and IBN-10

The Prizm-AN measurement installation comprises three primary components: (1) a non-boronated polyethylene prism featuring a horizontal channel; (2) an IBN-10 capsule radioisotope fast neutron source produced by Isotope (http://www.isotop.ru/); and (3) a scintillator radiometer-dosimeter, commonly referred to in Russia as the MKS-01R.

The calculation models of Prizm-AN and IBN-10 are illustrated in Figs. 4 and 5. The polyethylene prism (density of polyethylene is 0.945 g/cm^3), composed of C_2H_4, has a nuclide density of 11.98×10^{-2} nuclide/(b × cm). It is structured as a parallelepiped with dimensions of 90 cm in height, 89 cm in width, and 94.5 cm in depth (90 × 89 × 94.5 cm^3). Positioned 48 cm from the bottom edge, there is a horizontal rectangular channel measuring 13 cm in width and 12 cm in height, with a depth of 59.5 cm. This horizontal channel is filled with an air mixture, which has an atomic density of 4.99×10^{-5} nuclide/(b × cm).

The IBN-10 capsule neutron source, depicted in Fig. 4, has a cylindrical geometry characterized by a diameter of 3.50 cm and a height of 4.50 cm. The coordinates of the central part of the IBN-10 are as follows: x = 44.55 cm, y = 57.75 cm, and z = 50.25 cm. The active region of the capsule measures 2.70 cm in both diameter and height. This active component consists of a densely sintered mixture of $^{wg}PuO_2$ and beryllium powder, highlighted in red in Fig. 4c and 5.

The general technical parameters are presented in Table 1. The

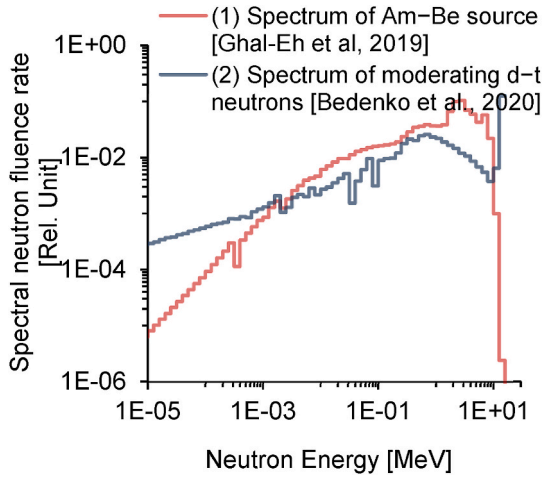

Fig. 3. Spectra of the Am−Be (Ghal-Eh et al., 2019) and plasma sources of the neutrons (Bedenko et al., 2020).

specific material composition of the IBN-10 active component is proprietary information of the manufacturer and is therefore not disclosed in this paper. It is important to note that the neutron emission characteristics of this capsule type are influenced by the mass ratio of the target material (*i.e.*, beryllium) to the radioactive nuclide (*i.e.*, plutonium). Considering that the average grain size of the PuO_2 crystals is approximately 3–5 μm, the optimal mass ratio of beryllium to plutonium is found to be in the range of 8:1 to 10:1.

The IBN-10 capsule features a double-encapsulated stainless-steel shell with a total density of 7.92 g/cm^3. Its composition by weight percentage is as follows: Fe (up to 67%), Cr (17–19%), Ni (9–11%), Mn (up to 2%), Ti (0.4–1%), Si (up to 0.8%), Cu (up to 0.3%), C (up to 0.12%), P (up to 0.035%), and S (up to 0.02%). The activity of the plutonium isotopes contained within the source is 250 GBq (approximately 6.8 Ci). According to the manufacturer (http://www.isotop.ru/), the capsule emits approximately 1.00×10^7 neutrons per second isotropically (into 4π steradians), a value that has been experimentally determined to represent the (I_n^{exp}) strength of the fast neutron source.

The point-to-point emission spectrum of unmoderated (α, n) neutrons from the IBN-10 source, normalized to 10^6 α particles, is calculated in the Nedis-3 code (see the applications of the code in Bedenko et al., 2020; Vlaskin et al., 2021; Rahmani et al., 2022; Vlaskin et al., 2023) and presented in Fig. 6a. The corresponding group spectrum, displayed in Fig. 6b ($\int dN/dE = 1$), and the emission neutron yield ($Y_n = 9.03 \times 10^6$ n. s^{-1}, see Table 1) was reconstructed under the condition that the experimental (according to the manufacturer, Table 1) I_n^{exp} and calculated values of the I_n^{Nedis} fast neutron source strengths are equal. When calculating the neutron yields and their spectra in Nedis, the fine-grained structure of the active part of the capsule was considered.

Then, we used Nedis code to calculate the effective dose rate based on this spectrum (blue curve in Fig. 6b), utilizing the fluence-to-dose coefficients for the anterioposterior exposure geometry listed in ICRP Publication 116 (ICRP, 2010).

The calculated fluence-to-dose conversion coefficient from the spectrum (blue curve in Fig. 6b) to an effective dose rate is DF = 1.58 μSv × h^{-1}/(n·cm^2). The DF coefficient is a convenient conversion factor for a quick estimate of the dose rate at a desired point in space. In this estimation, we neglect the geometry of the source and the change in its spectrum. To compare the results of the calculation according to Nedis-3 with the works (Vega-Carrillo et al., 2002; Peleshko et al., 2019; Rusnak and Vykydal, 2021; Pyshkina et al., 2021), the dose rate ($\dot{H}^*(10)$) was calculated with coefficients [pSv × cm^2] for the ambient dose (ICRP, 1996). The obtained ambient dose equivalent rate $\dot{H}^*(10)$ in this way, at a distance of 1 m from the IBN-10 source, is equal to 141.6 μSv × h^{-1}, and with a relative error of ≤15 % (most likely, due to the differences in the geometry between the IBN-10 and IBN-25) corresponds to the data published in the Peleshko et al. study (Peleshko et al., 2019).

The data on the spectrum of Pu–Be sources declared by the International Organization for Standardization (ISO) are incomplete. However, the (α, n) neutron spectra of Pu–Be and Am–Be sources are similar (Vega-Carrillo et al., 2002; Vega-Carrillo and Martinez-Ovalle, 2016). Therefore, the reconstructed emission spectrum (blue curve in Fig. 6b) was validated by comparing it with the neutron spectrum from an Am–Be source (red curve in Fig. 6b) recommended by ISO 8529-1 (International Organization for Standardization, 2021). Comparing the spectra shown in Fig. 6b, it is clear that the energy distributions of neutrons with energies above 3 MeV are very similar. However, for energies below 3 MeV, there is a slight difference. According to ISO 8529–1, the spectrum of the Am–Be source contains more low-energy neutrons compared to the Pu–Be source. This difference can be explained by the moderation of neutrons due to elastic and inelastic scatterings on the structural elements of the Am–Be capsule. It has been established that, within a relative error of ±15%, the neutron component of dosimetric characteristics such as ambient dose equivalent rates and neutron fluence rates of IBN-10 corresponds to the published data

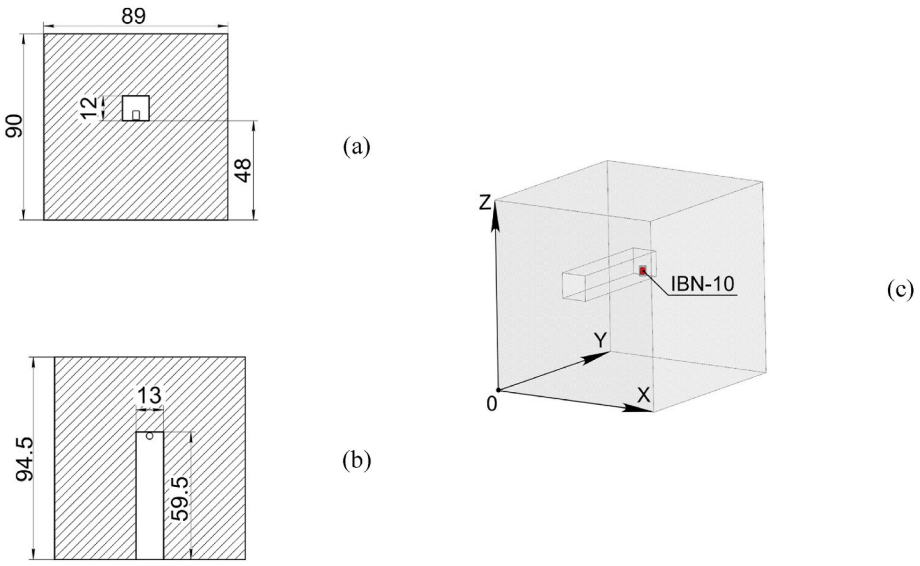

Fig. 4. Calculation model of Prizm-AN and IBN-10: (a) x-z plane, (b) x-y plane, (c) 3D Prizm-AN configuration with IBN-10 capsule. Dimensions are in cm.

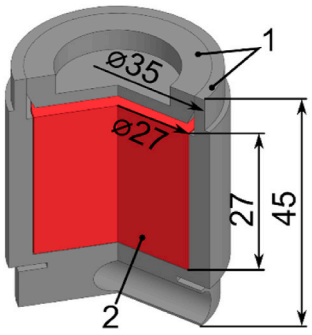

Fig. 5. Capsule neutron source of type IBN-10 (dimensions are in mm): (1) steel capsule; (2) the active part of the capsule.

Table 1
General technical parameters of Pu–Be source.

Parameters	Value
Fast neutron source strength in 4π steradians [n. s^{-1}]	$(1.00 \pm 0.10) \times 10^7$
Neutron emission yield (this work simul.) [n. s^{-1}]	9.03×10^6
Mass of ^{239}Pu [g]	2.94
Mass of plutonium isotopes [g]	3.31
Activity of plutonium isotopes [GBq/Ci]	250/6.8
Fluence-to-dose conversion coefficient (This work simul.) [μSv × h^{-1}/(n. cm^2)]	1.58
Date of neutron flux measurement	May 20, 2022
Outer dimensions [cm]	
Diameter	3.5
Height	4.5
Dimensions of the active part [cm]	
Diameter	2.7
Height	2.7
Capsule material according to Russian classification	Double-encapsulated stainless-steel grade 12X18N10T

(Peleshko et al., 2019; Vega-Carrillo and Martinez-Ovalle, 2016). Thus, the comparison results confirm the correctness of the calculated data sets obtained in Nedis-3, which are used further in the second step of the research.

The spatial and energy characteristics of the neutron field, along with the dose parameters of the Prizm-AN system equipped with the IBN-10 capsule, were computed using the Serpent 2.1.32 software (ENDF/B VII.1) (NEA, 2024; Serpent, 2015), as depicted in Fig. 4c. Neutron transport simulations were performed using an iterative method (Serpent, 2015). In each iteration, the spatial-energy distribution of neutrons within the IBN-10 and Prizm-AN materials was generated. The initial neutron distribution for initiating the iterative process was based on the source data, as illustrated in Fig. 6b (blue curve).

To assess the distribution of neutron fluence rate along the axial direction (*i.e.*, vertically along the height of the prism), we employed a detector capable of measuring this parameter in 720 discrete layers, each separated by a distance of 0.125 cm. Similarly, to quantify the neutron fluence rate in the radial direction (*i.e.*, within the horizontal channel of the prism), we positioned a detector that subdivided the channel and its polyethylene extension into 756 equal segments. This fine spatial resolution enabled us to generate a sufficiently smoothed visual representation of the results in both axial and radial directions while adhering to acceptable standards for statistical precision, as indicated by the standard deviation.

The technical support of the TENIS and its maintenance in the operating mode requires an assessment of the dose load created by Prizm-AN with the IBN-10 capsule installed inside. To determine the dosimetric characteristics, we employed a cubic water phantom with side lengths of 5 cm. This size of the phantom ($5 \times 5 \times 5$ cm^3), which is as close as possible to human tissue in terms of properties, ensured a statistically significant result. The phantom was positioned at distances ranging from 0 to 100 cm from the frontal plane of the Prizm-AN, aligned coaxially with the horizontal channel. Subsequently, a direct calculation of the effective dose rate for photons was performed using the specialized ENDF/B VII.1 library (NEA, 2024). The effective dose rate for neutrons was calculated utilizing the fluence-to-dose conversion coefficients listed in ICRP Publication 116 (ICRP, 2010).

2.3. TENIS and artificial neural networks with MATLAB

In a previous study (Bagherzadeh-Atashchi et al., 2023), it was demonstrated that the thermal neutron images reconstructed by TENIS can serve as input data for accurately unfolding the neutron spectrum from both mono- and poly-energetic neutron sources.

To unfold the energy spectrum of unknown neutron sources using the ANN toolbox in MATLAB, we constructed a response matrix for TENIS based on data from 70 pixels derived from reconstructed images. This dataset was acquired when TENIS was exposed to 109 mono-energetic neutron beams, spanning neutron energies from 10^{-11} to 14.92 MeV

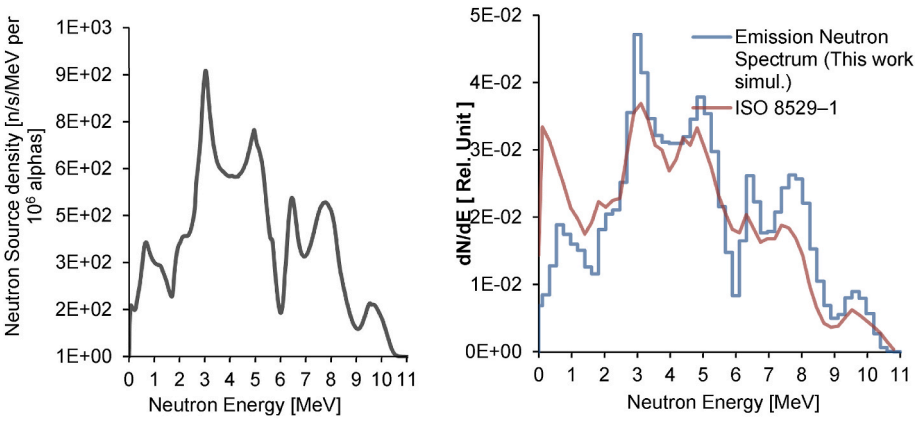

Fig. 6. Neutron spectra of IBN-10: (a) the point-to-point spectrum of emission α-n neutrons normalized by 10^6 α-particles; (b) the corresponding group spectrum and the spectrum of Am–Be source neutrons (International Organization for Standardization, 2021).

in equi-lethargy energy intervals. For the creation and training of the ANN, we employed a driver script developed in MATLAB (Bagherzadeh et al., 2023). Furthermore, TENIS was exposed to a neutron fluence rate of $\varphi = 1.10 \times 10^3$ n/(cm^2.s) in the spectrum of which there were $\varphi_{<0.5eV} = 5.66 \times 10^2$ n/(cm^2.s) thermal neutrons, leading to the acquisition of 70-pixel thermal neutron images, which were subsequently utilized for neutron spectrometry through ANN unfolding.

The neural networks developed for neutron spectrum unfolding feature three layers, comprising two hidden layers and one output layer, as illustrated in Fig. 7. The Levenberg-Marquardt (Yang et al., 2021; Hagan et al., 2014; Rojas, 2013; Feldkamp et al., 2001) backpropagation algorithm was utilized for training these networks, and the ANN Toolbox in MATLAB was employed for implementation. The transfer functions for the neurons in both the hidden and output layers were defined using the hyperbolic tangent sigmoid function (tansig).

To assess the comparison between the actual spectrum and the ANN-unfolded spectrum across multiple energy intervals, we utilized the root-mean-square error (RMSE) and the correlation coefficient (R^2) as evaluation metrics. The RMSE and R^2 values were calculated using the equations outlined in the works of Pham et al. and Bagherzadeh et al. (Pham et al., 2020; Bagherzadeh-Atashchi et al., 2023):

$$RMSE = \sqrt{\frac{1}{m}\sum_{j=1}^{m}\left(\phi_E(E)_j^{ANN} - \phi_E(E)_j^{Actual}\right)^2} \quad (1)$$

$$R^2 = 1 - \frac{\sum_{j=1}^{m}\left(\phi_E(E)_j^{ANN} - \phi_E(E)_j^{Actual}\right)^2}{\sum_{j=1}^{m}\left(average\ of\ \phi_E(E)_j^{ANN} - \phi_E(E)_j^{Actual}\right)^2} \quad (2)$$

The optimal architecture of the ANN was identified by selecting the configuration that produced the lowest RMSE and the highest R^2.

3. Results and discussion

3.1. Radiation characteristics of the Prizm-AN installation with the IBN-10 capsule

The spatial and energy distributions of the neutron field within the prism volume are depicted in Figs. 8 and 9. Fig. 8a illustrates the total neutron fluence rate in the x-y plane of the Prizm-AN installation. The dotted line indicates the geometry of the horizontal channel housing the IBN-10 capsule. The radial distribution of thermal (10^{-10} to 5×10^{-7} MeV), epithermal (5×10^{-7} to 0.1 MeV), and fast neutrons (0.1–20 MeV) in the y-z coordinates (with the z-axis oriented perpendicular to the frontal plane of the prism) is illustrated in Fig. 8b. The distribution of the neutron fluence rate is characterized by a pronounced asymmetry. This is because the high-density polyethylene array in the radial direction opposite to the prism channel direction has good moderating and diffusion properties. Moderation, diffusion and leakage of neutrons lead to the formation of thermal and epithermal signatures in the polyethylene part of the Prizm-AN installation. The significant variability of the fast neutron fluence rate in the horizontal channel of the prism can be largely attributed to the geometric attenuation of the flux which follows the dependence $\varphi \sim 1/R^2$. For epithermal neutrons, the influence of both the geometry and material of the prism was not noticeable because the field in this energy range was formed mainly by neutron scatterings. The relatively high thermal neutron fluence rate and its non-uniform distribution result from the moderation and diffusion processes occurring within the prism material, which leads to a return of neutrons into the channel due to thermal neutron albedo (reflection coefficients).

The comparison results of the calculated and experimental values of the neutron fluence rate show a good agreement over the entire length of the collimator channel (Fig. 8b, $\varphi_{<0.5\ eV}$). The maximum uncertainty did not exceed 20%.

The calculated value of the neutron beam, defined as the number of neutrons passing through the cross-section of the prism channel with an

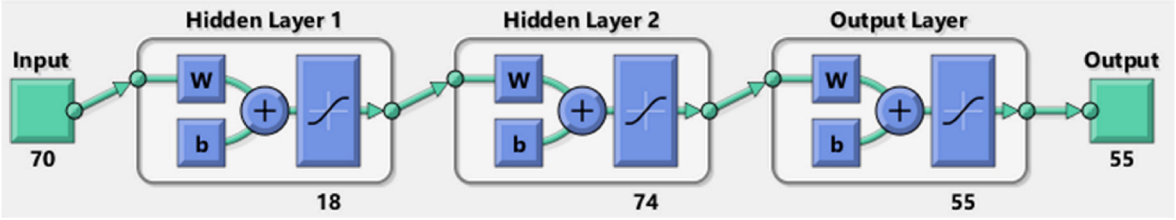

Fig. 7. The ANN architecture used for unfolding the neutron spectrum.

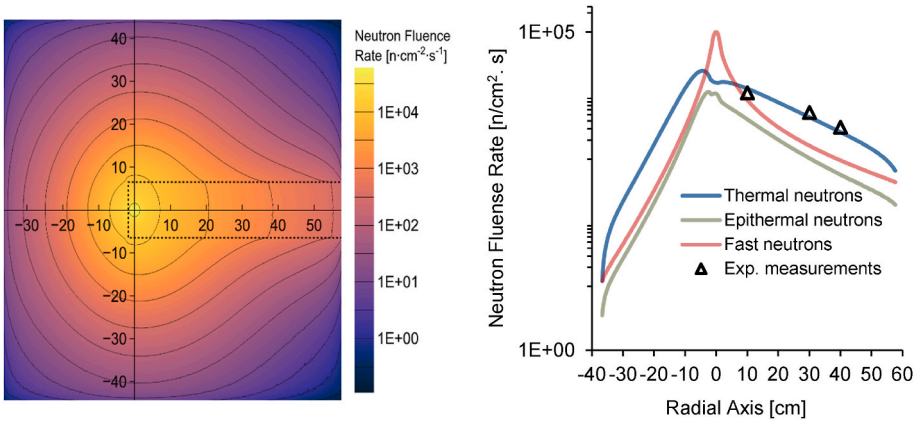

Fig. 8. Spatial distribution of the neutron field: (a) distribution of the neutron fluence rate over the xy-section of Prizm-AN; (b) radial distribution of the neutron fluence rate.

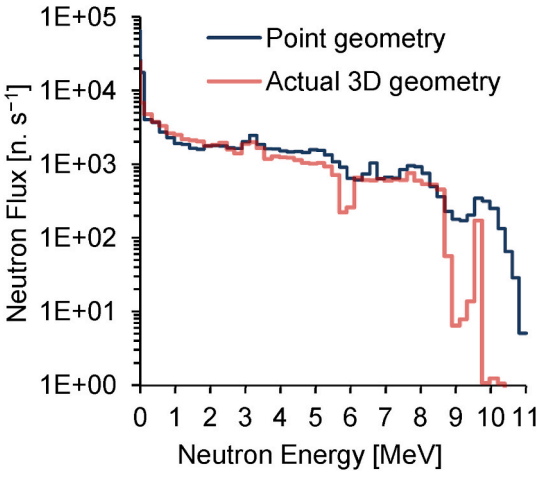

Fig. 9. Neutron beam spectrum in the Prizm-AN channel for point and actual geometry of IBN-10.

area of 156 cm^2 per unit time, is approximately 1.61×10^5 n. s^{-1}. This corresponds to a neutron fluence rate of approximately 1.10×10^3 n/(cm^2.s) (Table 2), reflecting the emission rate from the source. The energy distribution of these neutrons is depicted in Fig. 9. The solution data illustrated in Fig. 9 is obtained for the point and actual 3D-configuration of the IBN-10 capsule. The result of comparing the energy spectra in Fig. 9 with each other and with the initial emission spectrum (blue line in Fig. 5b) allows us to conclude that the neutron beam in the facility channel consists mainly of (α, n) neutrons, as well as of the reflected and scattered components of the neutron field. The observed signature at the end of the spectrum is probably a moderated part of the corresponding high-energy peak of the emission neutron spectrum.

The neutron field data (Figs. 8 and 9 (red line)) obtained at this stage will serve as the input data for the TENIS framework and ANN.

The technical support and maintenance of the TENIS system during operation require an evaluation of the radiation dose generated by the Prizm-AN device when the IBN-10 capsule is installed. In accordance with recommendations from the International Commission for Radiological Protection (ICRP, 2007), Group A personnel must adhere to a dose regime where the average effective radiation dose does not exceed 20 millisieverts [mSv] over any five-year period, with a maximum yearly exposure limit of 50 mSv. Given that operations occur annually, it is advisable to further restrict the cumulative dose to a maximum of 20 mSv per year. Utilizing data obtained on effective dose rates at varying distances from the Prizm-AN installation, we calculated the permissible duration of exposure for personnel throughout the year (Table 2).

Table 2
Permissible exposure limits for operations near the horizontal channel of the Prizm-AN.

Distance from the Prizm-AN [cm]	Effective Dose Rate [μSv × h^{-1}]		Neutron Fluence Rate [n. cm^{-2} × s^{-1}]			Permissible operating time [h]
	Photon	Neutron	$\varphi_{<0.5\ eV}$	$\varphi_{0.5\ eV-0.1\ MeV}$	$\varphi_{0.1-20\ MeV}$	
0	9.17	504	565.75	183.90	348.89	39.0
20	3.59	252	110.03	55.52	157.65	78.3
40	1.95	144	49.35	31.96	91.84	137.0
100	0.64	36	15.41	9.78	34.80	546.9

3.2. TENIS detection system and ANN unfolding of neutron flux

The image data of TENIS when it is exposed to the Prizm-AN beam is given in Fig. 10. These data were fed into MATLAB's ANN. Fig. 11 illustrates the unfolded results and the corresponding measured values.

The performance of the ANN in unfolding the neutron energy spectra of the Prizm-AN neutron beam was evaluated using the calculated

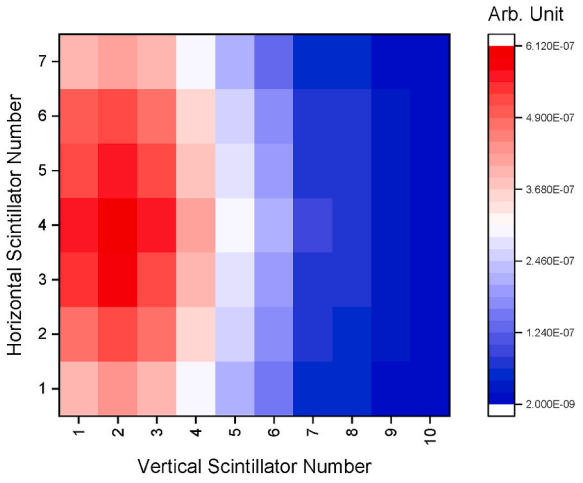

Fig. 10. The reconstructed 2D thermal neutron map of TENIS when it is exposed to Prizm-AN neutrons.

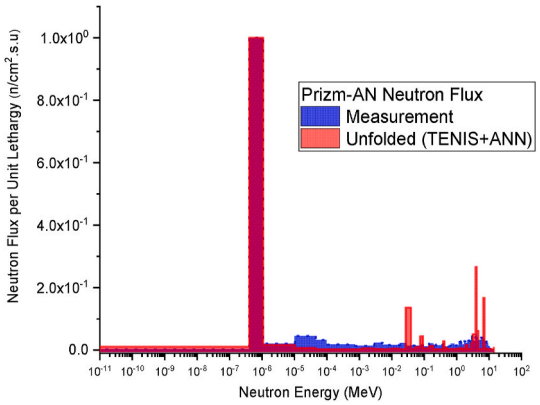

Fig. 11. ANN-unfolded neutron spectrum of Prizm-AN versus the measured results.

correlation coefficient and root-mean-square error (RMSE) values. The correlation coefficient (R^2) of 0.992 and RMSE value of 0.041 indicate a good agreement between the ANN-unfolded spectrum and the actual measurements. Additionally, the R^2 value, combined with the low RMSE, further underscores the high quality of the proposed spectroscopy system and unfolding procedure.

4. Conclusions

This study examines the use of TENIS for characterizing the spectrum of an (α, n) neutron flux produced in the collimated channel of the Prizm-AN installation utilizing an IBN-10 source.

At the first stage of the study, the Nedis-3 software code performed a computational estimation of the neutron spectrum (Table 1, Fig. 6) produced by a Pu–Be radioisotope capsule of the IBN-type with a total activity of 250 GBq (approx. 6.8 Ci). The results of the comparison, with an uncertainty of less than 15%, confirmed the accuracy of the calculated data sets obtained in Nedis-3. These data sets were then used in the second stage of the study.

In the second stage, numerical modeling was performed using the Serpent 2.1.32 software code to simulate the radiation properties of Prizm AN with IBN-10 capsule. The calculations show that, at $I_n = 10^7$ n. s^{-1}, the neutron fluence rate at the output of the damp window was 1.1 $\times$ 10^3 n/(cm^2.s) (Table 2). The comparison of calculated and experimental data shows good agreements throughout the length of the collimate channel, with a maximum uncertainty of 20% for the neutron fluence rate. The corresponding neutron flux value, defined as the number of neutrons crossing the cross-sectional area of the prismatic channel per unit time and equal to 156 cm^2, is approximately 1.61 $\times$ 10^5 n. s^{-1}. Note that the spectrum of these neutrons (Fig. 9) contains approximately 51.5% thermal neutrons, 16.74% epithermal neutrons, and 31.76% fast neutrons.

Finally, the study showed that diagnostic equipment of TENIS effectively visualized the (α, n) flux with parameters achieved in a collimated horizontal channel in Prizm-AN, as illustrated in Fig. 10, and a detailed map of neutron flux was created. The spectrum was unfolded and visualized (Fig. 11), using ANN tools in MatLab. R^2 of 0.992 and a low RMSE emphasized the high quality of both the spectrometry system and procedure for ANN-unfolded neutron spectrum parameters.

Furthermore, the study results reveal that the neutron spectrum generated by the PSN, particularly in the epithermal energy range, closely resembles that of the IBN-10 capsule. This observation allows for a comparative analysis between the ^{2,3}H fusion- and the (α, n) reactions, suggesting a potential synergy between the Prizm-AN and TENIS systems for investigating the technical capabilities of the coupled blanket-PSN-vBSA system in the pre-design phase of the demonstration version. In this context, the Prizm-AN and TENIS complex serves as a viable analogue for monitoring the parameters of D-T plasma emanating from the PSN.

Future investigations at the Prizm-AN facility will aim to validate the use of TENIS diagnostic tools for monitoring PSN plasma parameters and neutron flux through both computational and experimental approaches.

CRediT authorship contribution statement

S. Bedenko: Writing – original draft, Software, Methodology, Investigation, Data curation, Conceptualization. **S. Polozkov:** Visualization, Software, Investigation. **G. Vlaskin:** Writing – review & editing, Validation, Methodology, Data curation, Conceptualization. **N. Ghal-Eh:** Writing – original draft, Software, Methodology, Investigation, Conceptualization. **F. Rahmani:** Writing – review & editing, Methodology, Investigation, Conceptualization. **D. Veretennikov:** Visualization. **S. Bagherzadeh-Atashchi:** Visualization, Software, Investigation.

Declaration of competing interest

The authors declare that they have no known competing financial interests or personal relationships that could have appeared to influence the work reported in this paper.

Acknowledgments

This research was supported by the Russian Science Foundation under RSF grant No. 23-29-00131 (https://rscf.ru/en/project/23-29-00131/).

We would like to express our gratitude to the reviewers for their careful reading of the manuscript and thoughtful comments.

Data availability

Data will be made available on request.

References

Aza, E., Dinar, N., Manessi, G.P., Silari, M., 2016. A bonner sphere spectrometer for pulsed fields. Radiat. Protect. Dosim. 168 (2), 149–153. https://doi.org/10.1093/rpd/ncv180.

Bagherzadeh-Atashchi, S., Ghal-Eh, N., Rahmani, F., Izadi-Najafabadi, R., Bedenko, S.V., 2023. Neutron spectroscopy with TENIS using an artificial neural network. Appl. Radiat. Isot. 201, 111035. https://doi.org/10.1016/j.apradiso.2023.111035.

Bedenko, S.V., Polozkov, S.D., Demin, A.S., Ghal-Eh, N., Rahmani, F., & Vega-Carrillo, HR. Neutron pumping of active medium formed by gadolinium isotopes ^{155}Gd and ^{156}Gd pair: A feasibility study. Appl. Radiat. Isot. 206, 111232. https://doi.org/10.1016/j.apradiso.2024.111232.

Bedenko, S.V., Vlaskin, G.N., Ghal-Eh, N., Lutsik, I.O., Irkimbekov, R.A., Rahmani, F., Vega-Carrillo, H.R., 2020. Nedis-Serpent simulation of a neutron source assembly with complex internal heterogeneous structure. Appl. Radiat. Isot. 160, 109066. https://doi.org/10.1016/j.apradiso.2020.109066.

Bedenko, S.V., Lutsik, I.O., Prikhodko, V.V., Matyushin, A.A., Polozkov, S.D., Shmakov, V.M., Vega-Carrillo, H.R., 2022. Fusion-fission hybrid reactor with a plasma source of deuterium-tritium neutrons in a linear configuration. Prog. Nucl. Energy 154, 104477. https://doi.org/10.1016/j.pnucene.2022.104477.

Borgwardt, T.C., Bartlett, K.D., Smith, K., Meierbachtol, K.C., 2022. A compact neutron spectrometer system. Nucl. Instrum. Methods Phys. Res. 1027, 166202. https://doi.org/10.1016/j.nima.2021.166202.

Buffler, A., Comrie, A., Hutton, T., 2023. A compact direction-sensitive fast neutron spectrometer. Nucl. Instrum. Methods Phys. Res. 1052, 168256. https://doi.org/10.1016/j.nima.2023.168256.

Feldkamp, L., Feldkamp, T., Prokhorov, P., 2001. Neural network training with the nprkf. In: International Joint Conference on Neural Networks'01, pp. 109–114. https://doi.org/10.1109/IJCNN.2001.939001.

García-Baonza, R., Lorente, A., Ibáñez, S., Lacerda, M.A.S., Machado, I., Gallego, E., García-Fernández, G.F., Cevallos-Robalino, L.E., Vega-Carrillo, H.R., 2023. Comparison of extended-range and conventional Bonner Sphere Spectrometers (BSS) in an AmBe neutron field – applicability of the ReBUNKI unfolding code for extended-range BSS. Radiat. Phys. Chem. 203, 110647. https://doi.org/10.1016/j.radphyschem.2022.110647.

Ghal-Eh, N., Green, S., 2016. A plastic scintillator-based 2D thermal neutron mapping system for use in BNCT studies. Appl. Radiat. Isot. 112, 31–37. https://doi.org/10.1016/j.apradiso.2016.03.002.

Ghal-Eh, N., Rahmani, F., Bedenko, S.V., 2019. Conceptual design for a new heterogeneous ^{241}Am-^{9}Be neutron source assembly using SOURCES4C-MCNPX

hybrid simulations. Appl. Radiat. Isot. 153, 108811. https://doi.org/10.1016/j.apradiso.2019.108811.
Hagan, M.T., Demuth, H.B., Beale, M.H., De Jesús, O., 2014. Neural Network Design, p. 800. Martin Hagan.
Heshmati, K., Ghal-Eh, N., Najafabadi, R.I., Vega-Carrillo, H.R., 2022. Gamma-ray energy spectrum unfolding of plastic scintillators using artificial neural network. Appl. Radiat. Isot. 186, 110265. https://doi.org/10.1016/j.apradiso.2022.110265.
ICRP, 1996. Conversion coefficients for use in radiological protection against external radiation. ICRP publication 74. Ann. ICRP 26 (3–4).
ICRP, 2007. Conversion coefficients for use in radiological protection against external radiation. ICRP Publication 103. Ann. ICRP 37 (2–4).
ICRP, 2010. Conversion Coefficients for use in Radiological Protection against External Radiation. ICRP Publication 116. Ann. ICRP 40, 2–5.
International Organization for Standardization, 2021. Reference Neutron Radiations - Part 1: Characteristics and Methods of Production, vols. 8529–1. ISO.
Ivanov, A.A., Prikhodko, V.V., 2013. Gas-dynamic trap: an overview of the concept and experimental results. Plasma Phys. Contr. Fusion 55 (6), 063001.
Nuclear Energy Agency, Evaluated Nuclear Data Library Descriptions. < https://oecd-nea.org/-dbdata/data/nds_eval_libs.htm > [Reviewed October 2024].
Peleshko, V.N., Savitskaya, E.N., Sannikov, A.V., 2019. ^{239}Pu–Be-Source based neutron reference fields. At. Energy. 126, 313–319. https://doi.org/10.1007/s10512-019-00556-8.
Pham, B.T., Singh, S.K., Ly, H.B., 2020. Using artificial neural network (ANN) for prediction of soil. Vietnam Journal of Earth Sciences 42 (4), 311–319.
Pyshkina, M.D., Vasilyev, A.V., Ekidin, A.A., 2020. A neutron spectrum reconstruction for purposes of personnel dosimetry: Modelling study. In: Simos, T.E., Kalagiratou, Z., Monovasilis, T. (Eds.), International Conference of Computational Methods in Sciences and Engineering 2020. ICCMSE [040011] (AIP Conference Proceedings; 2343). American Institute of Physics Inc.
Rahmani, F., Ghal-Eh, N., Bedenko, S.V., 2022. Landmine-identification system based on the detection of scattered neutrons: a feasibility study. Radiat. Phys. Chem. 199, 110264. https://doi.org/10.1016/j.radphyschem.2022.110264.
Rojas, R., 2013. Neural Networks: a Systematic Introduction. Springer Science & Business Media, p. 502.
Rusnak, Jan, Vykydal, Zdenek, 2021. Determination of a Pu-Be source neutron spectrum at Czech Metrology Institute. Appl. Radiat. Isot. 175, 109786. https://doi.org/10.1016/j.apradiso.2021.109786, 2021.
Shamanin, I.V., Kazaryan, M.A., 2017. Nuclide kinetics involving hafnium and gadolinium nuclei in long–lived isomeric states. Bull. Lebedev Phys. Inst. 44, 215–217. https://doi.org/10.3103/S1068335617070077.
Shamanin, I.V., Kazaryan, M.A., Bedenko, S.V., Knyshev, V.V., Shamanin, V.I., 2021. Neutron pumping of active medium formed by gadolinium isotopes Gd^{155} and Gd^{156} pair. Appl. Radiat. Isot. 171, 109649. https://doi.org/10.1016/j.apradiso.2021.109649.
Serpent, 2015. Serpent 2 Monte Carlo Code version 2.1.31 [online]. https://www.oecd-nea.org/tools/abstract/detail/nea-1923/ [Reviewed October 2024].
Vega-Carrillo, H.R., Martinez-Ovalle, S., 2016. Few groups neutron spectra, and dosimetric features, of isotopic neutron sources. Appl. Radiat. Isot. 117, 42–50. https://doi.org/10.1016/j.apradiso.2016.03.027.
Vega-Carrillo, H.R., Manzanares-Acuña, E., Becerra-Ferreiro, A.M., Carrillo-Nuñez, A., 2002. Neutron and gamma-ray spectra of ^{239}PuBe and ^{241}AmBe. Appl. Radiat. Isot. 57 (2), 167–170. https://doi.org/10.1016/S0969-8043(02)00083-0.
Vlaskin, G.N., Bedenko, S.V., Ghal-Eh, N., Vega-Carrillo, H.R., 2021. Neutron yield and energy spectrum of ^{13}C(alpha,n)^{16}O reaction in liquid scintillator of KamLAND: a Nedis-2m simulation. Nucl. Eng. Technol. 53 (12), 4067–4071. https://doi.org/10.1016/j.net.2021.06.023.
Vlaskin, G.N., Bedenko, S.V., Polozkov, S.D., Ghal-Eh, N., Rahmani, F., 2023. Neutron and gamma-ray signatures for the control of alpha-emitting materials in uranium production: a Nedis2m-MCNP6 simulation. Radiat. Phys. Chem., 110919 https://doi.org/10.1016/j.radphyschem.2023.110919.
Yang, B., Chen, Y., Guo, Z., Wang, J., Zeng, C., Li, D., Shu, H., Shan, J., Fu, T., Zhang, X., 2021. Levenberg-Marquardt backpropagation algorithm for parameter identification of solid oxide fuel cells. Int. J. Energy Res. 45 (12), 17903–17923. https://doi.org/10.1002/ER.6929.
Yazdandoust, H., Ghal-Eh, N., Firoozabadi, M.M., 2021. TENIS—ThErmal neutron imaging system for use in BNCT. Appl. Radiat. Isot. 176, 109755. https://doi.org/10.1016/j.apradiso.2021.109755.